Check for updates

On-site marine oil spillage monitoring probes formed by fixing oxygen sensors into hydrophobic/oleophilic porous materials for early-stage spotty pollution warning†

Yuxin Shi,[a] Yong Xu,[b] Fei Jiang,[a] Zhijuan Sun,*[a] Gang Wang, [b] Zhixiang Zeng, [b] Congjie Gao,[a] Qunji Xue[b] and Lixin Xue [id] *[a]

In this study, an efficient on-site marine oil spillage monitoring probe was developed by fixing oxygen consumption sensors into hydrophobic/oleophilic oil-absorbing porous materials. The impact of thickness and characters of the porous materials, the types of spilled oil, and the presence of salts and vibration in water on the parameters of the obtained signals was investigated. The probe could be used to detect the various representative types of spilled oils including lubricating oil, corn oil, soybean oil, *n*-hexane, petroleum ether and toluene, even in simulated sea water vibrating at different levels, having over 33 times reduced reliable low detection limit (RLDL) in detecting soybean oil in water (from 36.5 g L^{-1} to 1.1 g L^{-1}). The response time and signal-to-noise ratios (SNRs) of the probe varied greatly with the dynamic absorbing speed and oxygen barrier property of the spilled oils in the porous material, respectively. The probe showing the highest SNR of 190 dB for a 50 g L^{-1} on-site soybean oil spillage and the fastest response time of 9 s for a 50 g L^{-1} on-site toluene spillage in water may potentially be used as a key component in near-shore marine oil spillage monitoring systems to provide early-stage pollution warning.

Introduction

Oils such as petroleum oils, animal oils and plant oils had served as key energy sources for human beings, but at the same time oil spillage pollution has become a long-standing concern around the world.[1–5] Oil spillages can not only cause huge economic losses but also lead to significant ecological damage, resulting in pollution seriously impacting humans and terrestrial organisms.[6–10] Oil pollution could lead to growth stagnation, decrease in population, increased mortality, and reduced reproduction.[11–14] Therefore, a series of measures must be taken to monitor and deal with oil spillages in time.[15]

Currently, most oil spillage monitoring techniques are based on remote sensing technologies[13] including hyper-spectral remote sensing and active microwave sensing effective for monitoring large-area oil spillages.[16–21] Optical sensors used in

hyper-spectral remote sensing have wavelengths of visible light and infrared light, while microwave sensors used in active microwave sensing have longer wavelengths of microwaves.[22–27]

Hyper-spectral remote sensing uses the wavelengths of ultraviolet (100–400 nm), visible (400–700 nm), and near-infrared (750–1400 nm) lights.[28–32] Optical images containing unique spectral characteristics of spilled oil from the pollution space could provide valuable information to differentiate oil spills from the blooms of algae. However, such monitoring depends greatly on weather conditions and the levels of sunshine.[33–35]

Microwave sensors used microwave radar technology, which can collect oil spillage data at any time of the day and under any weather conditions, independent of cloud coverage, providing a wider range of uses.[36,37] However, the biggest challenge of using synthetic aperture radar images from remote microwave sensing technologies comes from interference with a variety of man-made or natural objects such as plankton, fish, algae, wave, and air turbulence.[34,36,38–40]

Most of these on-line remote sensing techniques using very expensive devices had added a lot of cost to the oil spillage monitoring work. Lower cost off-line oil spillage monitoring methods involving oil sample extraction and examination with ultraviolet (UV) absorption, infrared spectroscopy, weight measurement, and gas chromatography have been

[a] Center for Membrane Separation and Water Science & Technology, College of Chemical Engineering, Zhejiang University of Technology, Hangzhou, Zhejiang 310014, PR China. E-mail: xuelx@zjut.edu.cn

[b] Key Laboratory of Marine Materials and Related Technologies, Zhejiang Key Laboratory of Marine Materials and Protective Technologies, Ningbo Institute of Materials Technology and Engineering, Chinese Academy of Sciences, Ningbo, Zhejiang 315201, PR China

developed.[41,42] The UV absorption method can only detect limited types of oils with low consistency, while the gas chromatography method needs to prepare the oil sample through long processes including dissolution, centrifugation, and chromatographic separation. Infrared spectroscopy is not conducive to direct measurement in the field and subject to a lot of human influence. Therefore, most offline oil spillage monitoring methods are high in labor cost with large potential error.[43]

Recently, comprehensive oil spillage monitoring systems have been established by our colleagues in China based on remote state-of-the-art sensing technologies involving satellites, air-crafts and ships for large-area oil spillage pollution control, but we are still lacking low-cost, efficient, real-time, on-site monitoring probes to generate early warning signals for sudden oil spillages at an initial spotty stage.[44–47] For this purpose, herein, the feasibility of developing on-site monitoring probes to detect marine oil spillages is based on hydrophobic and oleophilic porous materials and a fit-in oxygen consumption sensor, which is investigated to detect small-scale near-shore spotty marine oil spillages at their early stages. The hydrophobic and oleophilic porous materials including polypropylene non-woven fabrics (PP NWF) and polyurethane (PU) sponges should be low in cost and have appropriate pore size, porosity and hydrophobicity to pick up spilled oils from water. Such probes were constructed by fixing an oxygen consumption sensor into hydrophobic/oleophilic oil-absorbing porous materials, whose detection capacity is based on the changes in oxygen concentration inside the porous materials when its internal pores were filled with spilled oil. Signal parameters including response time, peak height, peak width and peak area were extracted from the differential curves. The impact of porous materials, spilled oil, and external environmental factors in water on the monitoring results was systematically investigated.

Materials and methods

Materials and equipment

PP NWF (Material A) was purchased from Clean & Environmentally Technology, Jiangsu, which was non-woven fabric made of 100% polypropylene. Superhydrophobic/ superoleophilic PU (polyurethane) sponge (Material B) was obtained from the team of Ningbo Institute of Materials Technology & Engineering.[48] PU sponge (Material C) was available from the local material market. PDMS (polydimethylsiloxane)-modified PU sponge (Material D) was prepared from PU sponge in house using the following process of hydrophobic and oleophilic modification: PDMS (0.1 g), curing agent (0.1 g), and ethyl acetate (100 mL) were mixed and dissolved in a beaker under stirring, and then hydrophobic silica (0.25 g) was added in to disperse. The PU sponge was dipped in this suspension and dried in a desiccator. After several repetitions, it was placed in an oven at 95 °C for 4 h.

Soybean oil, corn oil, and lubricating oil were purchased from a local market, petroleum ether and toluene were purchased from Shanghai Lingfeng Chemical Reagent Co., Ltd, *n*-hexane was purchased from Tianjin Yongda Chemical

Table 1 Property of hydrophobic/oleophilic materials

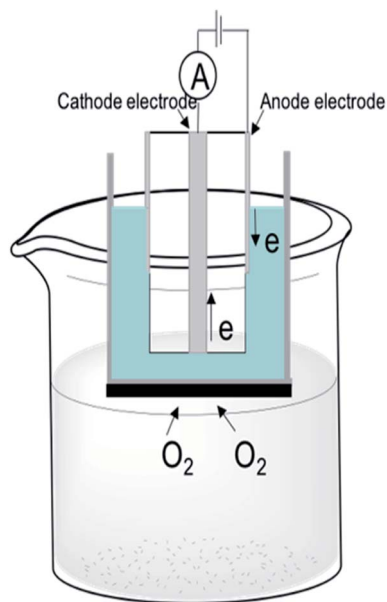| Materials	Material texture	Pore size (µm)	Porosity (%)	WCA (°)	Photo	Dynamic oil absorb speed (% s^{-1})
A	100% PP (polypropylene) NWF (non woven fabric)	100–200	50	144		12
B	Superhydrophobic–superoleophilic polyurethane sponge	250–500	88	152		4
C	Polyurethane sponge	200–570	80	135		7
D	Polyurethane sponge (PDMS modified)	200–570	80	144		6

Fig. 1 Reaction mechanism of an oxygen consumption sensor.

Reagent Co., Ltd, Na$_2$SO$_3$ (Sodium sulfite anhydrous) was obtained from Shanghai Macklin Biochemical Co., Ltd, and sea crystal was obtained from Jiangxi Yantong Co., Ltd Vibrator was obtained from Kamas store. The oxygen consumption sensor was obtained from Shanghai Haiheng Electromechanical Instrument Co., Ltd (Model: JPB-607), and the vibrator was purchased from Kamas Co., Ltd with 15 levels of settings (Model: 017A-3).

Characterization of materials

Water contact angles (WCAs) of the materials were tested using a contact angle tester (Germany Dataphysics OCA50AF/ OCA15EC), and the average porosity values of the materials were measured using a Capillary Flow Porometer (Germany Porometer Porolux 500), and the results are summarized in

Table 1. Oil viscosity was measured using a viscometer from American Brookfield (Model: DV2t). The molecular weight of oil was measured using a Gel Permeation Chromatograph (American Agilent PL-GPC50).

Working mechanism of an oxygen consumption sensor

As shown in Fig. 1, the oxygen consumption sensor in this experiment worked according to polar-graphic methods that determined oxygen concentration in the solution by measuring the potential–time curve between the polarized electrodes during electrolysis.[49,50] The sensor contained a gold cathode and a silver anode immersed in a potassium chloride solution communicating oxygen gas in the external media through an oxygen-permeable membrane. The measured change in potential signal over time reflects the change in the oxygen concentration in the external media, and the following reactions occur at the electrodes:

$$\text{Cathode: } O_2 + 2H_2O + 4e \rightarrow 4OH^-$$

$$\text{Anode: } 4Cl^- + 4Ag - 4e \rightarrow 4AgCl$$

Oil spillage monitoring experiments

The experimental online oil spillage monitoring system, as shown in Fig. S1,† contained an oil detection probe constructed by sealing hydrophobic/oleophilic porous materials around an oxygen consumption sensor with para-film wrap, so one side of the materials was closely contacting the oxygen permeating membranes of the oxygen consumption sensor (Fig. 2b), leaving the other side exposed to objective media.

Oil spillage monitoring experiments were conducted according to the procedure illustrated in Fig. 2a, where 0.8 L of water was first taken in a 1 L beaker placed on a vibrator. An oxygen consumption sensor wrapped with porous materials was then turned on and stabilized in air for 3 minutes before immersion into water (Fig. 2a-2) in a beaker. After stabilization
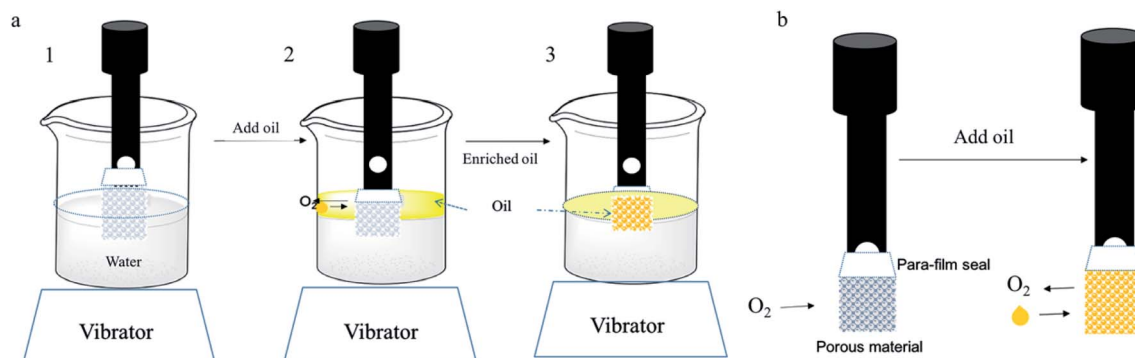

Fig. 2 (a) Schematic of the experimental procedure to monitor oil spillage using an on-site probe. (1) A probe with porous materials was immersed into 800 mL of water in a beaker without oil under vibration, where the oxygen signal detected was high. (2) Certain amount of oil was spilled into the water in the beaker, and the material began to absorb oil, where oxygen signal starts to drop. (3) All the pores of the porous materials were filled with the spilled oil, where oxygen signal detected were low. (b) Illustration of the change in oxygen concentration detected by the probe when oil was absorbed into the oleophilic porous materials.

for another 3 minutes, the vibrator was turned on to level 1. After the value of the oxygen concentration became stable, a certain amount of oils (1–50 mL) was quickly poured onto the water in the beaker and the value of the oxygen change was recorded every 3 second (Fig. 2a-3). Based on the detected change of oxygen concentration over time, a numerical change curve (oxygen concentration value dropping) and a differential curve with peak signals were obtained and reported. Each experiment was repeated 3 times to obtain the values of averages and relative standard deviations (RSD) for responding time, peak height, half width and peak area corresponding to the type and thickness of porous materials used, type of oil spilled, vibrator settings, and water salt content.

Data processing

Signal parameters such as peak height, peak width and peak area were extracted from the differential curve of the oxygen sensor using the SCIDAVIS software. The response time was defined as the time from the addition of oil to water to the peak point in a differential curve. Each result value was obtained from the average of results from at least 3 experiments. The SNRs for each parameter may be figured out following eqn (1):

$$SNR = \frac{H}{\sigma d} \qquad (1)$$

where H is the real parameter value obtained during the oil spillage and σd is the background noise standard deviation of the parameter values before adding oil.

Minimum RLDL determination

To obtain the minimum RLDL of the probe, the peak area values detected for 1 mL, 1.5 mL, 2 mL, 3 mL, 5 mL, 12.5 mL, 25 mL and 50 mL of soybean oil spilled into 800 mL of water were detected using an oxygen sensor probe several times. The signal peak area values from probe wrap with Material A were compared with those from the bare oxygen sensor without any wrapping. As summarized in Fig. 6 and Tables S3, S4,† δ_1 is the standard deviation of signal peak areas, δ_2 is the background standard deviation, δ_{1+2} is the sum of δ_1 and δ_2, and $3\delta_{1+2/max}$ is three times the maximum of δ_{1+2}.

The data were processed using the triple sigma rule,[50] which indicated that the detected peak area could be statistically valid if its average value was greater than $3\delta_{1+2/max}$. RLDL[51] of the probe for oil spillage was defined as the oil spillage amount corresponding to a peak area value of $3\delta_{1+2/max}$ figured out from the corresponding curve between peak area average values and oil spillage amounts in Fig. 7.

Dynamic oil adsorbing speed evaluation

Per experimental setup illustrated in Fig. S3 in the ESI,† porous materials were first cut into small squares of $4 \times 4 \times 0.3$ cm and

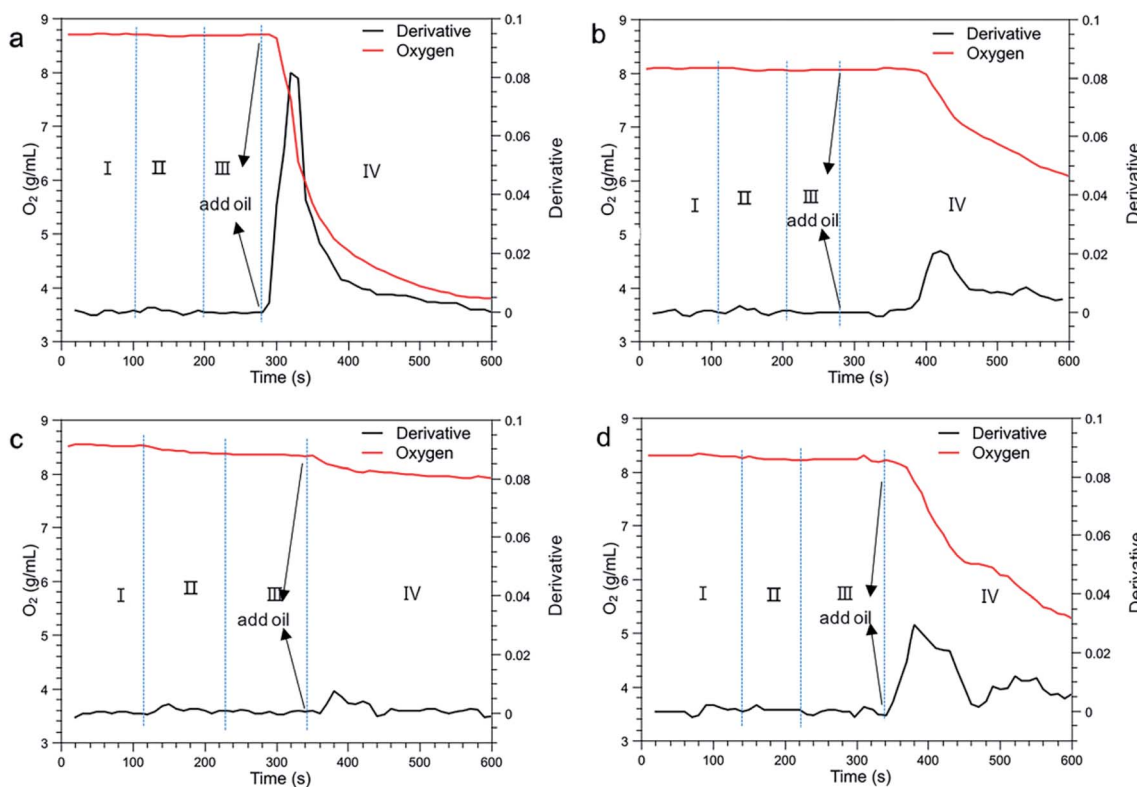

Fig. 3 Signals monitored using the oxygen consumption sensor probe fixed with various porous materials of 6 mm thickness for a 50 mL/0.8 L soybean oil spillage: (a) Material A, (b) Material B, (c) Material C and (d) Material D. (Zone I – the probe in air, Zone II – the probe in still water, Zone III – the probe in vibrated water, and Zone IV – the probe in water after a soybean oil spillage).

Table 2 Impact of porous materials on the response time and peak height SNRs of monitored soybean oil spillage peak signals

Material	Response time (s)	RSD (%)	Peak height	Back ground σd	Peak height SNRs (dB)
A	31 ± 1	2	0.080 ± 0.003	0.00042	190
B	48 ± 3	2	0.020 ± 0.002	0.00027	74
C	38 ± 3	8	0.0080 ± 0.0003	0.00057	14
D	43 ± 2	5	0.0300 ± 0.0008	0.00136	22

weighed (M_0), and then fixed horizontally to a glass rod mounted on an iron stand. Certain amount of oil was added on a Petri dish placed on a balance. The oil weight change (dW) in 12 s was recorded from the time when the glass rod was lowered to allow a slight direct contact between the porous material and the oil surface. Dynamic oil picking speed (S_a) can be calculated according to eqn (2):

$$S_a = \frac{100 \times dW}{M_0 \times 12} \qquad (2)$$

where S_a (% s^{-1}) is the dynamic oil absorb speed, dW is the oil weight change in 12 s, and M_0 is the weight of the virgin porous material. The results for the dynamic oil adsorbing speed of various materials to soybean oil and various oils to Material A are summarized in Tables S1 and S5 in the ESI,† respectively.

Results and discussions

Impact of porous materials on the monitored results

Characterization of hydrophobic/oleophilic porous materials. As shown in Fig. 2, the on-site oil spillage probe proposed was constructed by sealing hydrophobic/oleophilic porous materials around the oxygen consumption sensor with para-film wrap. One side of the porous material was contacting the oxygen consumption sensor, while the other side was exposed to the objective media. Due to the hydrophobic nature of the porous materials, water could not diffuse into the pores when the probes were placed into the water without oil spillage. Due

to the oleophilic nature of the porous materials, spilled oil could be quickly absorbed into the pores to let out the air to generate decreasing oxygen concentration signals for detection. Therefore, the porous materials used should have a high enough water contact angle value or hydrophobicity to prevent water permeation into the pores, and fast enough oil adsorbing kinetics to allow the rapid absorption of spilled water.

In this work, to test the feasibility of our on-site oil spillage detection concept, we have screened four types of hydrophobic/oleophilic porous materials for different pore sizes, porosities and water contact angle, as listed in Table 1, including PP NWF, superhydrophobic–superoleophilic PU sponge, PU sponge, and PDMF-modified PU sponge with water contact angles from 135 to 152°, a porosity ratio from 50 to 88%, and a pore size from 200 to 570 μm.

Influence of material types on monitored results. Signals monitored by the oxygen consumption sensor probe fixed with various porous materials of 6 mm thickness for a 50 mL/0.8 L (50 g L^{-1}) soybean oil spillage are shown in Fig. 3a–d respectively, where the red lines are the oxygen value change curves and the black line are their corresponding differential curves. The peak height, half width and peak area values of the differential curves are listed in Table S1 in the ESI,† while the results of comparison of response time and peak height SNRs are presented in Table 2.

From Table 2 and Fig. 4a, it is clear that PP NWF (Material A) with porosity ratio of 50% and pore size of 100–200 μm, showed
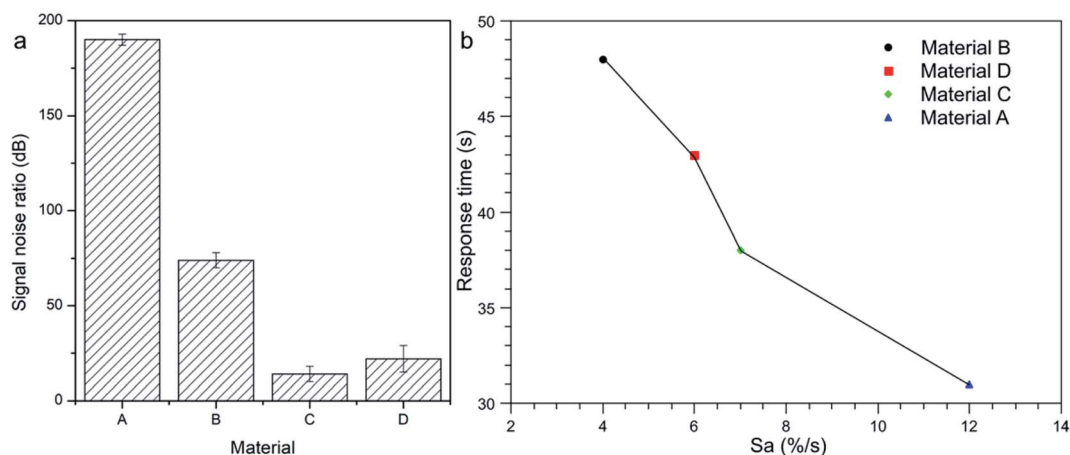

Fig. 4 (a) Influence of material types on the peak height SNRs of monitored soybean oil spillage peak signals, and (b) relationship between response time and dynamic oil absorbing speed (Table 1).
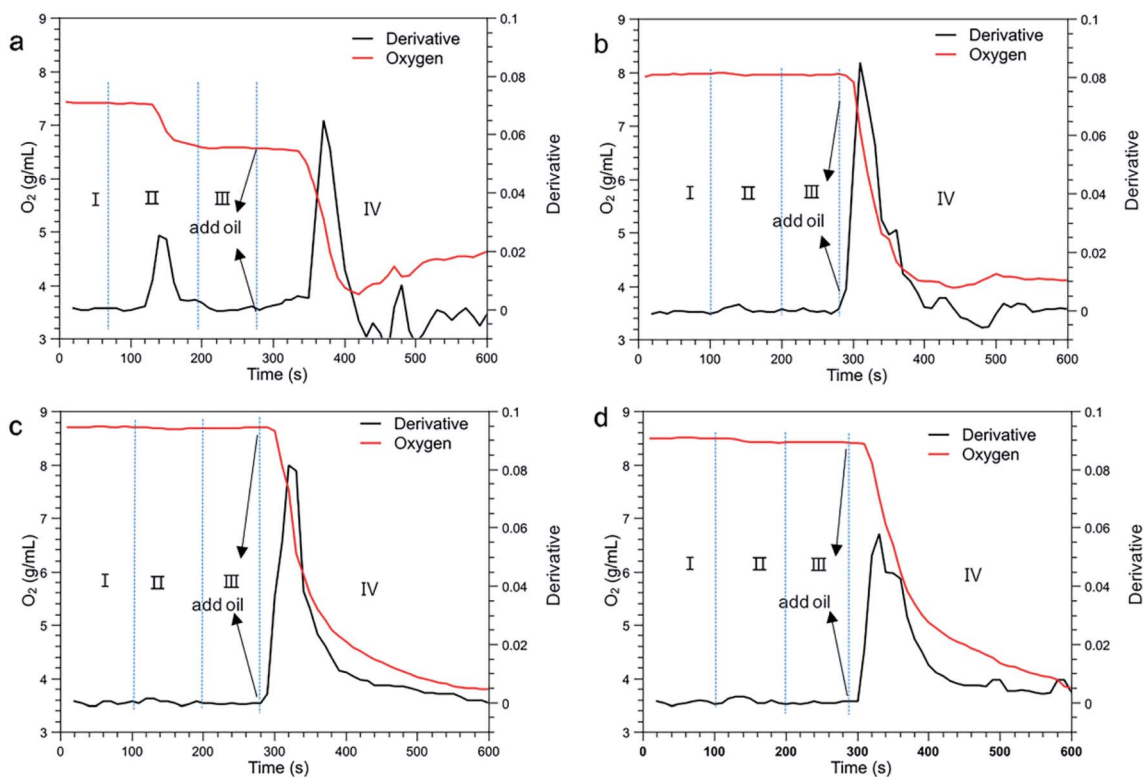
Fig. 5 Signals monitored by the oxygen consumption sensor probe fixed with (a) zero layer; (b) 1 layer; (c) 2 layers; and (d) 3 layers of Material A for a soybean oil spillage (50 mL/0.8 L) in fresh water. (Zone I monitoring signal of the probe in air, Zone II monitoring signal of the probe in still water, Zone III monitoring signal of the probe in vibrated water, and Zone IV monitoring signal of the probe in water after a soybean oil spillage.)

Table 3 Impact of the thickness of porous Material A on the response time and SNRs of monitored soybean oil spillage peak signals

PP NWF	Response time (s)	RSD (%)	Peak height	Back ground σd	Peak height SNRs (dB)
0	11 ± 1	9	0.08 ± 0.01	0.00082	97
1	22 ± 2	9	0.090 ± 0.002	0.00061	148
2	31 ± 1	3	0.080 ± 0.003	0.00042	190
3	40 ± 2	5	0.060 ± 0.003	0.00035	170

much higher SNRs (190) and shorter response time (31 s) than the PU sponge foams with higher porosity ratio (80–88%) and larger pore sizes (200–570 μm). Among the PU sponges, super-hydrophobic–superoleophilic PU sponge (Material B) showed the best repeatability (lowest RSD) due to its highest water contact angle, but with longer response time and lower peak SNRs due to slower adsorption kinetics from larger pore size (250–500 mm) and higher porosity ratio of 88%. PDMS-modified PU sponge (Material D) performed better than conventional PU (Material C) with lower RSD and higher SNRs because of its improved hydrophobicity (WCA 144°). The dynamic oil absorbing speeds of the materials are compared in Table 1, and from the plot in Fig. 4b, it is clear that the faster the oil absorbing speed, the shorter the response time.

In short, porous materials with WCA above 140°, a pore size of 100–200 μm, and a porosity ratio around 50% are preferred choices for this purpose. Although it was worth to do more
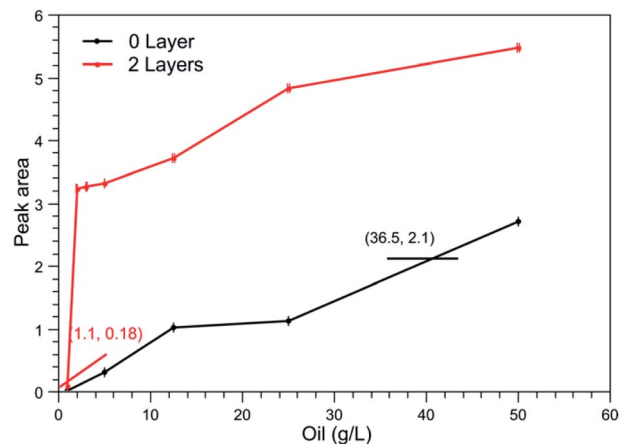

Fig. 6 Impact of soybean oil spillage level on the signal peak area values detected using the oxygen probe fixed with 2 layers of Material A.

detailed systematic studies on the influence of the chemical and physical characters of the porous materials on the parameters of the monitored signals in future, Material A was selected to do further study in this paper for its high SNRs and low RSD values. Materials with improved hydrophobicity and higher S_a may become better choices later.

Impact of the thickness of the porous material on the monitored results

Influence of the numbers of PP NWF layers. Each layer of PP NWF (Material A) was 0.3 mm thick, and hence, the thickness of the porous materials wrapped around the oxygen sensor may be varied by changing the number of layers of Material A. Signals monitored by the oxygen consumption sensor probe fixed from

0 to 3 layers of Material A are included in Fig. 5, while related signal parameters including peak height, half width and peak area and their standard deviation values are summarized in Table S2 in the ESI.† It showed that the probe with 2-layer Material A had the lowest RSD values, indicating the best repeating reliability.

The impacts of the thickness of porous Material A on the response time (RT) and SNRs of monitored soybean oil spillage peak signals are summarized in Table 3. Data in Table 3 clearly showed that as the number of layers of Material A increased from 0 to 3, the response time of the probe increased from 11 to 40 s, while the peak height SNRs increased from 97 DB to 190 DB at 2 layers and then dropped to 170 DB at 3 layers of Material A. When the oxygen sensor was fixed with the 0 layer of PP NWF, the SNR was lowest; on the contrary, when the sensor fixed 2
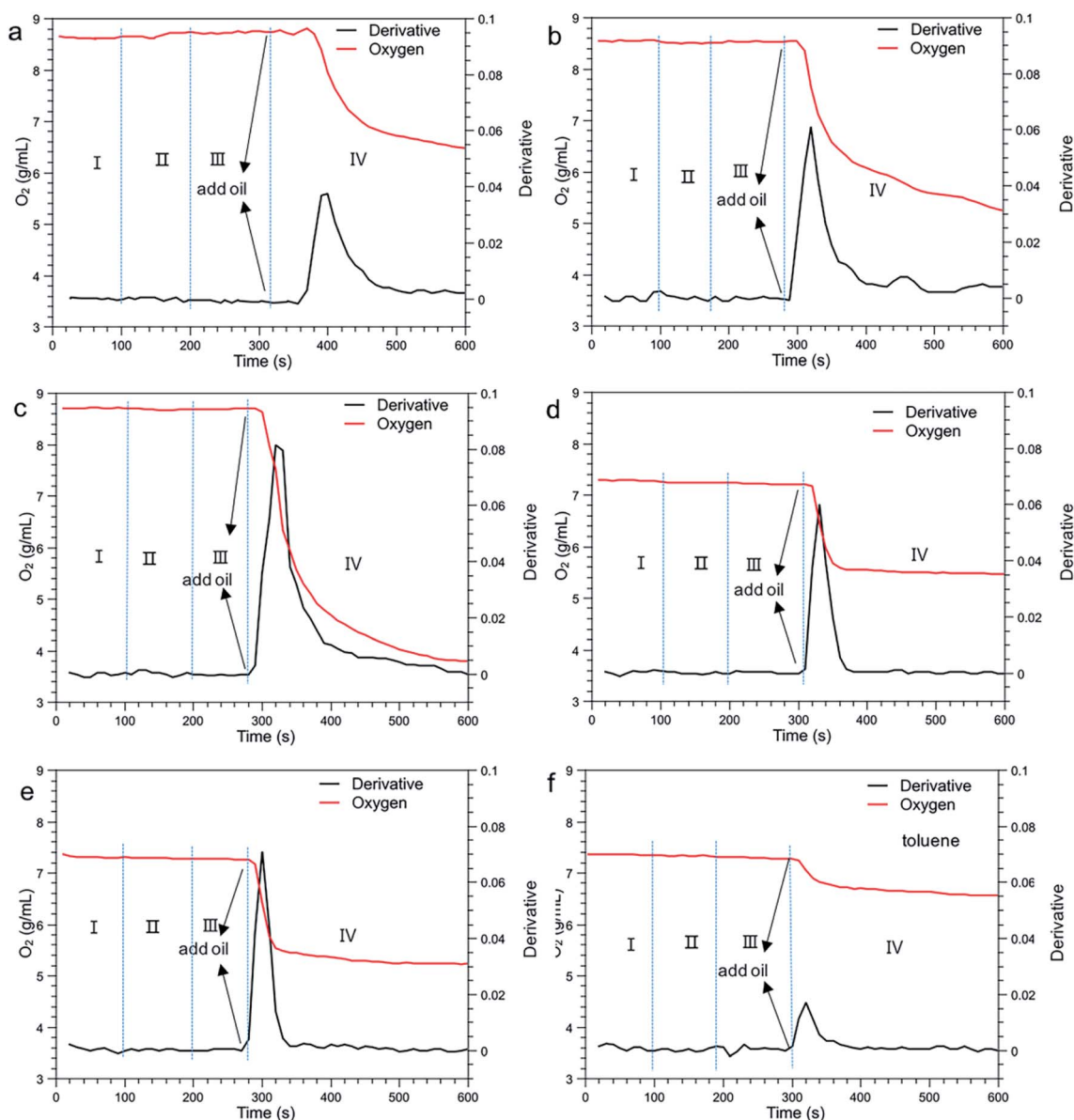

Fig. 7 Signals monitored by the oxygen consumption sensor probe fixed with 2 layers of Material A for varied types of oil spillage (50 mL/0.8 L) in fresh water: (a) lubricating oil; (b) corn oil; (c) soybean oil; (d) *n*-hexane; (e) petroleum ether; and (f) toluene.

Table 4 Impact of oil type on the response time and peak height SNRs on monitoring oil spillage in fresh water

Oily	Response time (s)	RSD (%)	Peak height	Back ground σd	Peak height SNRs (dB)
Lubricating oil	96 ± 1	1	0.040 ± 0.002	0.00044	100
Corn oil	44 ± 1	3	0.063 ± 0.002	0.00046	137
Soybean oil	31 ± 1	3	0.080 ± 0.003	0.00042	190
n-Hexane	14 ± 1	7	0.060 ± 0.001	0.00044	136
Petroleum ether	12 ± 1	8	0.0700 ± 0.0003	0.00042	166
Toluene	9 ± 1	11	0.020 ± 0.001	0.00048	41

layers of PP NWF, the SNR was highest. These results clearly indicated that wrapping with 2 layers of Material A (6 mm thickness) on the oxygen probe yields the most reliable and repeatable detection signals for soybean oil spillage.

When the sensor was not fixed with any porous materials, its oxygen permeating membrane contacted directly with water or oil to have the fastest response time. However, the external motion of water or oil had greatly influenced the monitoring process. In Fig. 5a, it is clearly observed that there was an obvious side peak in Zone II caused by the added vibration. This type of background peak caused by physical motion of water could severely interfere with oil spillage monitoring in Zone IV. Fortunately, in Fig. 5b–d, after porous Material A was wrapped onto the sensor as a barrier, this interfering peak could be greatly reduced.

Determination of minimum RLDL. Our data showed that the performance of three layers in Material A was no better than two layers in SNRs. With more layers of porous materials mounted on, longer response time was needed to reach the peak value in addition to unfavorable increase in size and material cost. Therefore, we chose to use 2 layers of Material A to continue our study to construct the probe for the on-site early-stage oil spillage warning system.

As demonstrated previously in Fig. 2a, major advantage of using hydrophobic/oleophilic porous material to wrap the oxygen sensor comes from its capability to absorb and enrich spotty and low level of soil pillage at the early stage. The essential character of an efficient on-site probe for rapid detection of spotty oil spillages at early stage is to have a reduced RLDL. The RLDL referred to the minimum concentration of spilled oil that may generate reliable and recognizable signals to lead to effective warning. Since uncertainty may come from the noise in the background and the duplicating error in the measurement procedure, at RLDL, the probe should generate signal values greater than three times the sum maximum of the standard deviation (SD) from background and duplicating experiments. Tables S3 and S4 in the ESI† showed the SD of the peak area values recorded when the sensor was fixed with or without 2 layers of PP NWF. δ_1 is the standard deviation of signal peak areas obtained from duplicating experiments, δ_2 is the standard deviations from the background without oil spillage, δ_{1+2} is the sum of δ_1 and δ_2, and $3\delta_{1+2/max}$ is three times the maximum of δ_{1+2}. The RLDL of the probe with and without 2 layers of PP NWF was figured out from Fig. 6 as 1.1 g L^{-1} and 36.5 g L^{-1}, respectively, indicating that the presence of the 2-layer PP NWF on the oxygen sensor had increased the detection capability of the probe over 33 times under the experimental setup.

Influence of spilled oil type on monitored results. The signals monitored by the oxygen consumption sensor probe
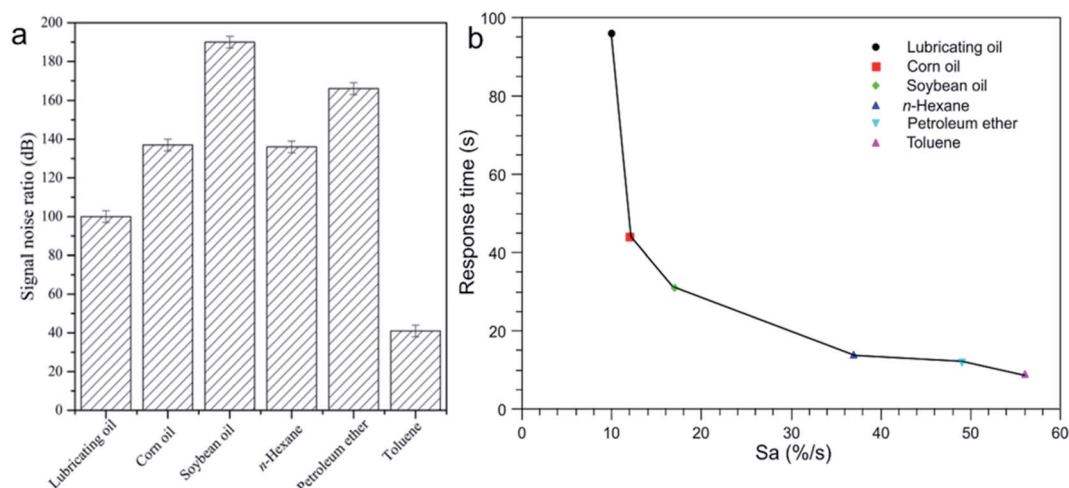

Fig. 8 (a) Influence of spilled oil types on the peak height SNRs of monitored oil spillage peak height signals detected by the oxygen probe fixed with 2-layer of Material A and (b) relationship between response time and dynamic oil adsorption speed (Table 5).

Table 5 Characteristics of different types of oils

Oil	MW	Viscosity (mPa s)	Polarity	Dynamic oil absorb speed (% s^{-1})
Lubricating oil	831	128	—	10
Corn oil	803	108	—	12
Soybean oil	320	108	—	17
n-Hexane	86	0.33	0.06	37
Petroleum ether	195	0.3	0.01	49
Toluene	92	0.59	2.4	56

fixed with 2 layers of Material A for six representative types of spilled oil in fresh water are compared in Fig. 7, while their peak parameter values were calculated, and the results are included in Table S5 in the ESI.† The corresponding response time and peak height SNRs results are shown in Table 4.

Due to the variation in oxygen barring capability of the spilled oils, the probe showed varied levels of responses after the adsorption of the spilled oil into the wrapping porous materials. The high oxygen barrier property required the oil to have low oxygen solubility and diffusion speed, leading to larger peak signals and higher SNRs. Generally, gas molecules such as oxygen molecules (O_2) tend to diffuse slower in more viscose oils such as lubricating oil, corn oil and soybean oil than *n*-hexane, petroleum ether and toluene, yielding higher SNRs for the former group, as shown in Fig. 8a. The oxygen barrier

property of oils is also influenced by their oxygen solubility, probably in the order of toluene > *n*-hexane > petroleum ether, and lubricating oil > corn oil > soybean oil, considering the electronic affinity of the O_2 molecules. The electron-rich aromatic carbon content in toluene and lubricating oils may provide hosting spots for electron-deficient O_2 molecules to permeate. Combining the solubility and diffusion factors, the final order of SNRs becomes toluene < lubricating oil < *n*-hexane < petroleum ether < corn oil < soybean oil, as shown in Table 4.

In Fig. 8b, it is demonstrated that the response time (RT) of oil was greatly relating to their oil absorbing kinetics in the porous material. From the result, RT seemed to decrease exponentially with the increase in S_a. According to Table 5, the S_a value of various oils absorbed into the PP NWF (Material A) was mainly controlled by their difference in viscosity. Therefore, more viscose oils tend to have a longer response time. Higher viscosity oils such as lubricating oil, corn oil and soybean oil showed a lower absorbing speed and a longer responding time (96–31 s) than low-viscosity *n*-hexane, petroleum ether and toluene (14–9 s).

Impact of environmental factors on the monitored results

Influence of the water vibration levels. In real marine environment, water motions caused by tides, waves, rains and winds are continuous interfering factors for oil spillage monitoring. Based on international standard of sea state rating, waves may be divided into ten grades, the moving patterns of sea water can
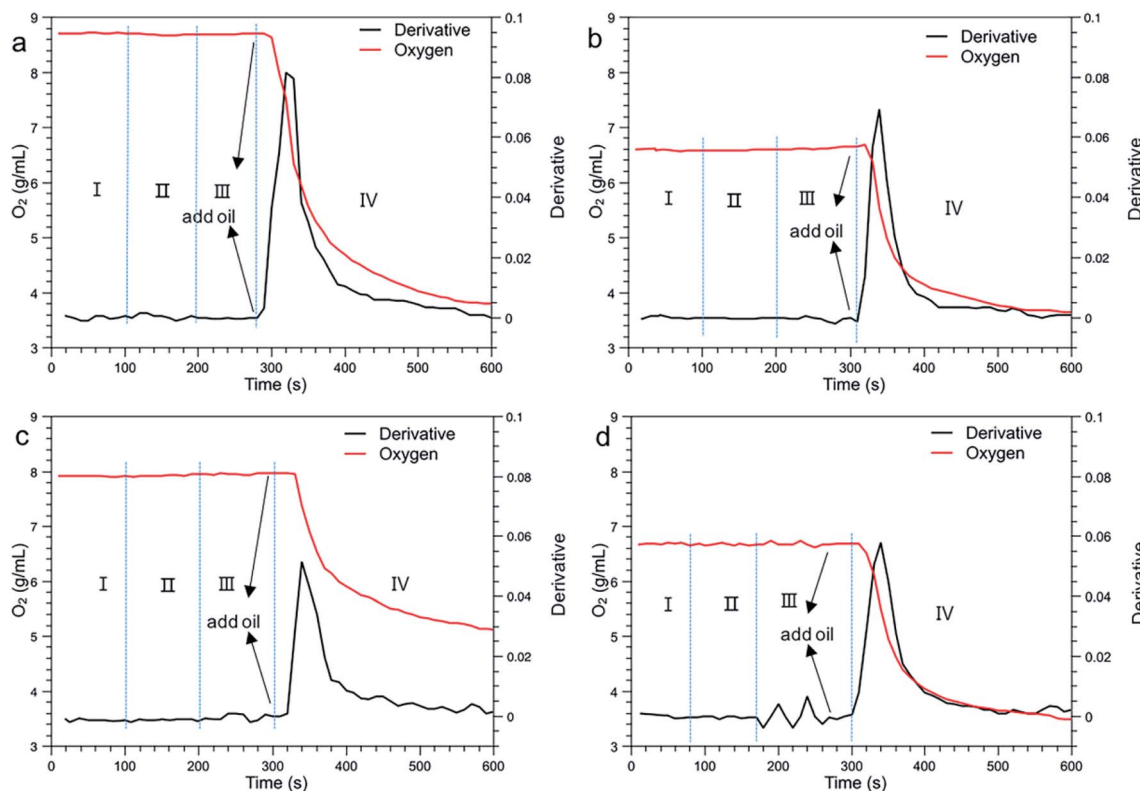

Fig. 9 Signals monitored by the oxygen consumption sensor probe fixed with 2 layers of Material A during a 50 mL/0.8 L soybean oil spillage under varied levels of vibration: (a) level 1; (b) level 5; (c) level 10; and (d) level 15.

Table 6 Impact of water vibration intensity on response time and peak height SNRs in monitoring oil spillage in fresh water

Degree of vibration	Response time (s)	RSD (%)	Peak height	Back ground σd	Peak height SNRs (dB)
1	31 ± 1	3	0.080 ± 0.003	0.00042	190
5	34 ± 1	3	0.070 ± 0.004	0.00072	97
10	48 ± 2	4	0.050 ± 0.001	0.001111	45
15	71 ± 4	6	0.056 ± 0.008	0.003294	17

be complicated and the moving speeds may vary in a wide range. In the experiments for on-site spillage monitoring, we first attempted to use a vibrator to simulate the effects of water motions. The levels of water motion here could be increased by changing the power setting level of the vibrator from 1, 5, 10, to 15. The signals monitored by the oxygen consumption sensor probe fixed with 2 layers of Material A during a 50 mL/0.8 L (50 g L^{-1}) soybean oil spillage under varied levels of vibration are shown in Fig. 9, while the relating peak parameters, response time, and SNRs are summarized in Tables 6 and S6 in the ESI.†

In Fig. 9, the effects of vibration level on peak heights and peak areas were quite distinct. When the vibration was higher, the peak height became smaller. As shown in Table 6, when the vibration intensity was increased from 1 to 15, the response time was increased from 31 s to 71 s, and the RSDs increased from 3% to 6%, while the peak height SNRs decreased from 190 dB to 17 dB. It is clear that the increased water vibration intensity has caused the increase in response time and RSD and decrease peak height and SNRs, leading to lower sensitivity and reliability. However, even under the highest vibration setting of 15, the SNRs of the signals were still maintained far above the statistically satisfied value 6 for meaningful detection. Overall, the probe had demonstrated great feasibility in detecting oil spillage in a moving water environment.

Influence of the salts in water on the monitored results. To test whether this probe could be used in the marine environment, we used sea crystals from a local fish market to prepare the simulated seawater solution with about 3.5% solid content for our study. The signals monitored under vibration setting 1 with soybean oil as a model oil using an oxygen consumption sensor wrapped with 2 layers of Material A are included in Fig. S3 in the ESI,† while their corresponding peak parameter, response time, and SNRs are summarized in Tables 7 and 8.

Comparing the salt water data in Table 7 with the fresh water in Table S5,† although the RSD values of all types of oil spillage in seawater were still maintained lower than 10%, the RSD values for toluene, petroleum ether and n-hexane were significantly increased in salted water, indicating less duplicating consistency. There are significant increases in peak area values of lubricating oil and decreases in peak area values of soybean oil and petroleum ether in the presence of salt in the water.

Comparing the salt water data in Table 8 with the fresh water data in Table 4, it was found that the response time of corn oil was significantly increased, with the peak height of SNRs going up for lubricating oil and n-hexane and going down for corn oil and soybean oil, respectively. The roles of salts in water can be complicated. They may accelerate separation of oil such as hexane from water by lowering the activity of water, at the same time interacting with some of the functional groups in other oils

Table 7 Signal parameters from spillages of varied types of oils (50 mL/0.8 L) into simulated seawater

Oils	Peak height	RSD (%)	Half width	RSD (%)	Peak area	RSD (%)
Lubricating oil	0.050 ± 0.001	2	31 ± 2	6	3.20 ± 0.10 (up)	3
Corn oil	0.050 ± 0.001	2	65 ± 2	3	2.90 ± 0.10	3
Soybean oil	0.060 ± 0.001	2	49 ± 3	6	3.40 ± 0.10 (down)	3
n-Hexane	0.070 ± 0.003	4	23 ± 1	4	1.90 ± 0.02	1
Petroleum ether	0.070 ± 0.005	7	35 ± 2	6	1.50 ± 0.10 (down)	7
Toluene	0.020 ± 0.002	10	20 ± 1	5	0.70 ± 0.06	9

Table 8 Response time and peak height SNRs of monitored signals from oil spillage in simulated sea water

Oil	Response time (s)	RSD (%)	Peak height	Back ground σd	Peak height SNRs (dB) in salt water
Lubricating oil	92 ± 4	4	0.050 ± 0.001	0.00058	86 (up)
Corn oil	59 ± 1 (up)	2	0.050 ± 0.001	0.00059	85 (down)
Soybean oil	35 ± 2	6	0.060 ± 0.001	0.00054	111 (down)
n-Hexane	14 ± 1	7	0.070 ± 0.003	0.00058	120 (up)
Petroleum ether	12 ± 1	8	0.070 ± 0.005	0.00055	128
Toluene	10 ± 1	10	0.020 ± 0.002	0.00057	35

to alter the absorbing speed and oxygen barrier property of the oils, for example, lubricating oil containing surfactants with carboxyl and sulfonate acid groups to interact with cations such as Na^+, Mg^{2+} and Ca^{2+} in seawater. Such interactions could lead to the formation of compounds with better oxygen barring capability, and hence larger peak area and SNR. The interaction of corn oil with salts in seawater may have decreased its absorbing speed by increasing its viscosity leading to increased response time. Although the reasons behind these results deserved further studies, it is demonstrated that oxygen sensors wrapped with hydrophobic/oleophilic porous materials could be used as effective probes to detect oil spillage in the marine environment with salted and moving water.

Conclusion

The feasibility of constructing an on-site probe for early-stage marine oil spillage monitoring by fixing an oxygen consumption sensor into oil-absorbing porous materials was demonstrated. Porous materials such as PP NWF wrapping could effectively eliminate the external background interference and enrich spilled oil from water, leading to over 33 times decrease in the RLDL. The response time and SNRs of the probe varied greatly with the dynamic absorbing speed and oxygen barrier property of the spilled oils in the porous material, respectively. External water vibration could reduce the monitored signal strength, extend the response time and increase the duplicating error, and salts in water may complicate the monitored results. Overall, the probe had demonstrated the great capability of detecting various representative types of spilled oils in simulated vibrating seawater and may be used as a key component to providing an effective warning for near-shore marine oil spillages at earlier stages.

Author contributions

Yuxin Shi: methodology, investigation, data curation, writing-original draft preparation. Yong Xu: methodology, materials, data curation. Fei Jiang: experiment, data curation, Zhijuan Sun: conceptualization, analysis. Gang Wang: methodology, resources. Zhixiang Zeng: machine, resources. Congjie Gao & Qunji Xue: resources. Lixin Xue: resources, methodology writing-original draft preparation, funding acquisition.

Conflicts of interest

There are no conflicts of interest to declare.

Acknowledgements

References

1 P. Li, Q. Cai, W. Lin, B. Chen and B. Zhang, *Mar. Pollut. Bull.*, 2016, **110**, 6–27.

2 O. Oliveira, A. Queiroz, J. Cerqueira, S. Soares, K. Garcia, A. Filho, M. Rosa, C. M. Suzart, L. Pinheiro and I. Moreira, *Mar. Pollut. Bull.*, 2020, **160**, 111597–111603.

3 A. Gokce Cicek Ceyhun, *Eur. Sci. J.*, 2014, **10**, 1857–7881.

4 S. E. Chang, J. Stone, K. Demes and M. Piscitelli, *Ecol. Soc.*, 2014, **19**, 26–50.

5 L. Goswami, R. Kumar, K. Pakshirajan and G. Pugazhenthi, *J. Hazard. Mater.*, 2019, **365**, 707–715.

6 D. Fustes, D. Cantorna, C. Dafonte, B. Arcay, A. Iglesias and M. Manteiga, *Future Generat. Comput. Syst.*, 2014, **34**, 155–160.

7 R. Sarbatly, D. Krishnaiah and Z. Kamin, *Mar. Pollut. Bull.*, 2016, **106**, 8–16.

8 M. G. Barron, D. N. Vivian, R. A. Heintz and U. H. Yim, *Environ. Sci. Technol.*, 2020, **54**, 6456–6467.

9 J. B. Culbertson, I. Valiela, M. Pickart and P. C. M. Reddy, *J. Appl. Ecol.*, 2008, **45**, 1284–1292.

10 L. Goswami, N. A. Manikandan, B. Dolman, K. Pakshirajan and G. Pugazhenthi, *J. Cleaner Prod.*, 2018, **196**, 1282–1291.

11 R. D. DeLaune, W. H. Patrick, J. W. Fleeger and M. D. Tolley, *Environ. Pollut., Ser. A*, 1984, **36**, 207–227.

12 K. A. Burns, *Estuarine Coastal Mar. Sci.*, 1979, **8**, 349–360.

13 I. B. Ivshina, M. S. Kuyukina, A. V. Krivoruchko, A. A. Elkin, S. O. Makarov, C. J. Cunningham, T. A. Peshkur, R. M. Atlas and J. C. Philp, *Environ. Sci.: Processes Impacts*, 2015, **17**, 1201–1219.

14 L. Goswami, R. Kumar, K. Pakshirajan and G. Pugazhenthi, *J. Cleaner Prod.*, 2020, **256**, 120253.

15 L. Goswami, N. A. Manikandan, J. C. R. Taube and K. Pakshirajan, *Environ. Sci. Pollut. Res.*, 2019, **26**, 25154–25166.

16 M. Fingas and C. Brown, *Mar. Pollut. Bull.*, 2015, **93**, 298–300.

17 M. Fingas, C. Brown and M. Fingas, *Oil Spill Sci. Technol.*, 2018, **18**, 91–108.

18 I. Leifer, W. J. Lehr, D. Simecek-Beatty, E. Bradley, R. Clark, P. Dennison, Y. Hu, S. Matheson, C. E. Jones, B. Holt, M. Reif, D. A. Roberts, J. Svejkovsky, G. Swayze and J. Wozencraft, *Rem. Sens. Environ.*, 2012, **124**, 185–209.

19 D. Casciello, T. Lacava, N. Pergola and V. Tramutoli, *Int. J. Rem. Sens.*, 2011, **32**, 4107–4129.

20 B. Zhang, W. Perrie, X. Li and W. G. Pichel, *Geophys. Res. Lett.*, 2011, **38**, 10602–10606.

21 S. Altobelli, M. Conradi, E. Fukushima, J. Hodgson, T. Nedwed, D. Palandro, A. Peach, N. Sowko and H. Thomann, *Mar. Pollut. Bull.*, 2019, **144**, 160–166.

22 S. T. Yekeen and A. L. Balogun, *Remote Sens.*, 2020, **12**, 3416–3446.

23 R. Al-Ruzouq, M. B. A. Gibril, A. Shanableh, A. Kais, O. Hamed, S. Al-Mansoori and M. A. Khalil, *Remote Sens.*, 2020, **12**, 3338–3339.

24 K. N. Topouzelis, *Sensors*, 2008, **8**, 6642–6659.

25 Y. Lu, X. Li, Q. Tian, G. Zheng, S. Sun, Y. Liu and Q. Yang, *Mar. Geol.*, 2013, **36**, 334–346.

26 Z. Zhong and F. You, *Comput. Chem. Eng.*, 2011, **35**, 1614–1630.

27 O. Garcia-Pineda, G. Staples, C. Jones, C. Hu, B. Holt, V. Kourafalou, G. Graettinger, L. DiPinto, E. Ramirez,

D. Streett, J. Cho, G. A. Swayze, S. J. Sun, D. Garcia and F. Haces-Garcia, *Rem. Sens. Environ.*, 2020, **236**, 111421–111435.

28 Y. Lu, S. Sun, M. Zhang, B. Murch and C. Hu, *J. Geophys. Res.: Oceans*, 2016, **121**, 148–161.

29 R. N. Clark, G. A. Swayze, I. Leifer, K. E. Livo, S. Lundeen, M. Eastwood, R. O. Green, R. F. Kokaly, T. Hoefen and C. Sarture, *U.S. Geological Survey*, Reston, 2010.

30 M. A. G. De Carolis and G. Pasquariello, in *Proceedings of the International Geoscience and Remote Sensing Symposium*, 2012, pp. 3002–3005.

31 G. Sicot, M. Lennon, V. Miegebielle and D. Dubucq, *GeoHyper*, 2015, **40**, 445–450.

32 J. Svejkovsky, M. Hess, J. Muskat, T. Nedwed, J. McCall and O. Garcia, *Mar. Pollut. Bull.*, 2016, **110**, 162–176.

33 E. A. Glinskis and V. H. Gutierrez-Velez, *Land Use Pol.*, 2019, **80**, 95–106.

34 M. Krestenitis, G. Orfanidis, K. Ioannidis, K. Avgerinakis, S. Vrochidis and I. Kompatsiaris, *Remote Sens.*, 2019, **11**, 1762–1783.

35 S. Sun and C. Hu, *IEEE Trans. Geosci. Remote Sens.*, 2019, **57**, 2643–2658.

36 J. Fan, F. Zhang, D. Zhao and J. Wang, *Maritime Oil Spill Response*, 2015, **3**, 112–118.

37 P. Genovez, N. Ebecken, C. Freitas, C. Bentz and R. Freitas, *Expert Syst. Appl.*, 2017, **81**, 384–397.

38 Y. Guo and H. Z. Zhang, *International Journal of Applied Earth Observation and Geoinformation*, 2014, **30**, 146–157.

39 P. Liu, C. Zhao, X. Li, M. He and W. Pichel, *Int. J. Rem. Sens.*, 2010, **31**, 4819–4833.

40 A. Solberg, *Proc. IEEE*, 2012, **100**, 2931–2945.

41 Q. Li and D. Yin, *Spectroscopy and Spectral Analysis*, 2019, **39**, 1661–1666.

42 G. Q. Wang, Q. Z. Ding and Z. Y. Hou, *TrAC, Trends Anal. Chem.*, 2008, **27**, 368–376.

43 Y. Lu, J. Liu, J. Ding, J. Shi, J. Chen and X. Ye, *Chin. Sci. Bull.*, 2019, **64**, 3213–3222.

44 Q. Xu, X. F. Li, Y. J. Wei, Z. Y. Tang and Y. C. Cheng, *Mar. Pollut. Bull.*, 2013, **44**, 107–116.

45 J. Liu and S. Zhu, *Energy Engineering and Environmental Engineering*, 2013, **580**, 316–317.

46 G. Lan, L. Ma and G. Chen, *Navigation of China*, 2011, **34**, 89–93.

47 G. Wang, Z. Zeng, X. Wu, T. Ren, J. Han and Q. Xue, *Polym. Chem.*, 2014, **5**, 5942–5948.

48 N. Razeghi, G. Jamshidinia and M. Hakimipour, *Iran. J. Public Health*, 1976, **5**, 46–47.

49 P. Cott, P. Sibley, A. Gordon, R. Bodaly, K. Mills, W. Somers and G. Fillatre, *J. Am. Water Resour. Assoc.*, 2008, **44**, 328–342.

50 W. Kenton, *Financial analysis*, 2020.

51 R. Bassy, P. Donfack and A. Materny, *J. Raman Spectrosc.*, 2009, **40**, 1284–1289.